



**HAL**  
open science

# Stratified spherical model for microwave imaging of the brain Analysis and experimental validation of transmitted power

M. Bjelogrljic, M. Volery, Benjamin Fuchs, J.-P. Thiran, J.R. Mosig, M. Mattes

## ► To cite this version:

M. Bjelogrljic, M. Volery, Benjamin Fuchs, J.-P. Thiran, J.R. Mosig, et al.. Stratified spherical model for microwave imaging of the brain Analysis and experimental validation of transmitted power. Microwave and Optical Technology Letters, 2018, 60 (4), pp.1042-1048. 10.1002/mop.31101 . hal-01739926

**HAL Id: hal-01739926**

**<https://univ-rennes.hal.science/hal-01739926>**

Submitted on 21 Jan 2021

**HAL** is a multi-disciplinary open access archive for the deposit and dissemination of scientific research documents, whether they are published or not. The documents may come from teaching and research institutions in France or abroad, or from public or private research centers.

L'archive ouverte pluridisciplinaire **HAL**, est destinée au dépôt et à la diffusion de documents scientifiques de niveau recherche, publiés ou non, émanant des établissements d'enseignement et de recherche français ou étrangers, des laboratoires publics ou privés.

# Stratified Spherical Model for Microwave Imaging of the Brain: Analysis and Experimental Validation of Transmitted Power

Mina Bjelogrić, Maxime Volery, Benjamin Fuchs, Jean-Philippe Thiran, Juan R. Mosig, and Michael Mattes

**Abstract**—This work presents the analysis of power transmission of a radiating field inside the human head for microwave imaging applications. For this purpose, a spherical layered model composed of dispersive biological tissues is investigated in the range of [0.5-4] GHz and is confronted to experimental verification.

**Index Terms**—Microwave Imaging, bio-medical applications, spherical wave expansion, 3D printed head phantom.

## I. INTRODUCTION

Microwave Imaging (MWI) [1] for bio-medical applications aims at localizing and reconstructing a pathological tissue region from scattered microwaves. In the framework of head MWI this non-invasive, non-ionizing technique is suitable to monitor brain anomalies such as brain stroke [2], internal bleeding, etc. Several main factors influence the quality of the MWI: the scattered power, the frequency and the medium in which the test object is immersed, called the matching or the background medium. The frequency is an essential parameter since all biological tissues are dispersive and the losses increase exponentially according to it.

Another important parameter is the spatial resolution of MWI which has a lower bound defined by the far field and only depends on the wavelength in the background medium. Devaney [3] first suggested that this limit of resolution was about  $\lambda/\sqrt{2}$ , then Bolomey and Pichot [4] estimated it to  $\lambda/2$ . Chen and Chew [5] experimentally observed a resolution up to  $\lambda/4$ , for high contrast, but non-dispersive and lossy objects,

which is a so-called super-resolution behavior, exploiting the near field and non-linear reconstruction algorithms. Meaney et al. [6] have suggested that image reconstruction “is fundamentally unlimited by wavelength” and “is restricted by signal-to-noise” ratio. The latter papers have been experimentally discussed by Semenov [7] and tested for the detection of myocardial ischemia and infarction. They concluded that the resolution lies between a quarter and a half of a wavelength in the background medium.

Several groups have developed complex imaging setups and algorithms for imaging brain anomalies [8] [9] [10] [11]. Experimental phantoms for the head have been developed, the most complex one using molded semi-rigid parts assembled inside an outer solid cavity [12]. The complex molding procedure and the high number of used ingredients makes this approach precise, however not easily repeatable. Moreover, the skin is not represented realistically as it is included in the fat/bone layer printed in a plastic material with dielectric constant of 6 at 2 GHz [13]. These models are very useful to realistically simulate the dielectric properties inside the brain itself and are used for imaging [9]. To validate numerical models, interesting works have been done in the microwave imaging community with a 3D printed breast phantoms [17] [18] with Triton X-100 based mixtures to mimic biological tissues. In the 7T MRI community 3D printed liquid phantoms [19] are also used as they are easy to handle and transportable. A similar approach is followed here, to our best knowledge, for the first time in the framework of MWI of the brain, and a first attempt of using this simple, repeatable and over time stable procedure was published recently in [20].

In [14] guidelines to design an optimal MWI setup and to properly set the working frequency and the matching medium, needed to facilitate the penetration of the probing wave into the head, are determined using a plane wave Transmission Line (TL) model since it allows a simple analysis. On the other hand, a multilayered spherical model better approximates the head geometry while still allowing an analytical solution to the electromagnetic scattering problem [15] [16].

This paper focuses on the analysis of the power transmission through the four main layers between the brain and the background medium, namely the Cerebrospinal Fluid (CSF), the bone, the fat and the skin. These four layers have very different influence on the propagation of the wave from and into the brain, according

to the frequency. For this, a spherically stratified head phantom has been built to experimentally estimate the power transmitted into the brain and to analyze the influence of these layers on the propagation of the EM wave.

## II. MODEL AND ELECTROMAGNETIC ANALYSIS

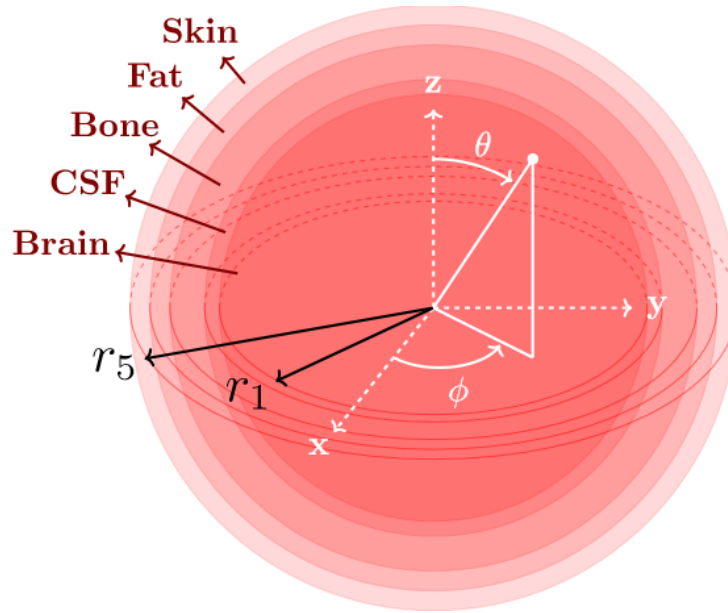


Figure 1: Spherical multilayered model to analyze the power transmitted into the human head.

The spherically stratified model, sketched in Fig. 1 (right), is a more realistic model of the human head than the planar model in [14] while still allowing an analytic solution for the electric field distribution. The core of the sphere is the brain with a radius of  $r_1 = 43\text{mm}$ , the  $j^{\text{th}}$  layer (the core is the  $1^{\text{st}}$  layer) is given by  $r \in [r_{j-1}, r_j]$ ,  $j = 2,3,4,5$ , and represents, respectively, the CSF (3mm), the cortical bone (7mm) (denoted here bone), the fat (4mm), the skin (4mm) and the matching medium (see Fig. 1). In [19] for 7T MRI the Larmor frequency is around 300MHz and the brain region is modeled as a combination of CSF, grey matter, and white matter. Since we deal with higher frequencies and, thus, shorter wavelengths, we model the CSF separately and the dielectric characteristics of the brain are set with a grey over white matter ratio (GM/WM

ratio) of 1.5 as shown in [21]. A similar ratio was used in [20], as the dielectric properties of the latter two are similar in the frequency range of interest.

Due to the spherical geometry of the boundary conditions, the electric field can be expanded as an infinite sum of vector spherical harmonics and be expressed analytically. Reference [22] provides a review on the governing equations of the spherical wave expansion used to solve this problem, and gives a detailed analysis and validations of the implementation. These results are valid for a plane wave impinging on the head phantom. This needs to be taken into account when comparing theoretical and experimental results. However, because we are only interested in the transmission inside the head, this is not a real restriction and the results using a plane wave should be also valid for an antenna directly placed on the head since the propagation of an electromagnetic wave depends only on the properties of the medium and not on the characteristics of the wave, that is plane wave, spherical wave, etc. Finally, we define the normalized transmitted power,  $P_{Nt}$ , as the ratio between the transmitted power into a bounded domain in the center of the brain and the power available in the lossless background in the very same bounded domain.

### C. Simulation Results and Discussion

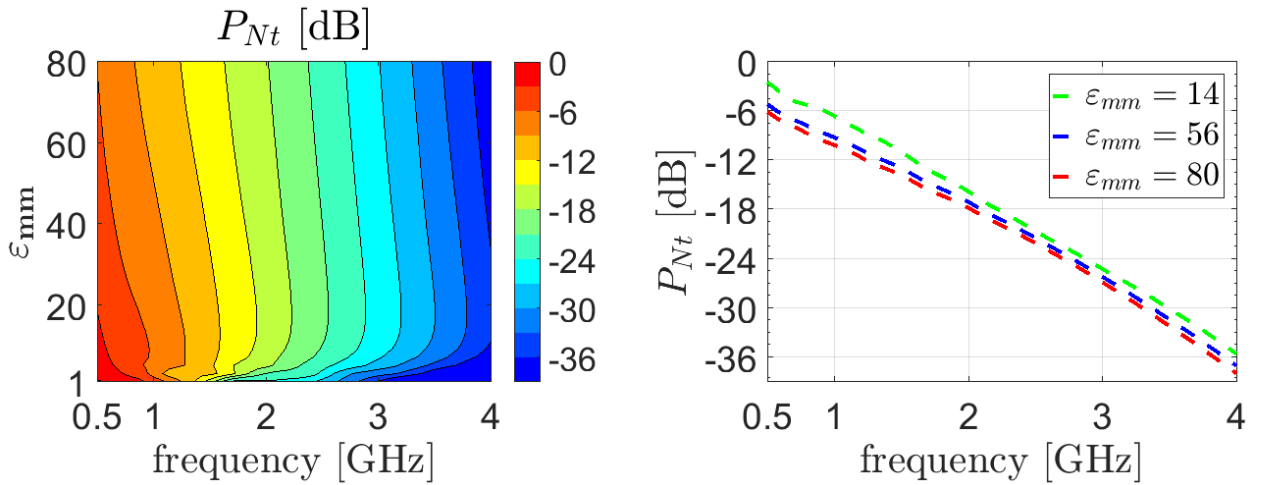


Figure 2: Normalized transmitted power according to the frequency [0.5 – 4]GHz, for a matching medium of  $\epsilon_{mm} = [1 - 80]$  (left). Cuts for  $\epsilon_{mm} = 14, 56, 80$  of the  $P_{Nt}$  (right).

The normalized transmitted power represents the incoming power that can excite any anomaly in the center of the head (worst case scenario) and therefore produce a scattered field. Fig. 2 represents a map of the

normalized transmitted power plotted in dB for the spherical (left) model. The permittivity of the matching medium is varying in the range  $\epsilon_{mm} = [1 - 80]$  (from air to water) and frequencies  $[0.5 - 4]$  GHz. The analysis is made for a lossless matching media as the conductivity has very small influence on the normalized transmission power [14]. The color change corresponds to a drop in the normalized transmitted power in steps of 3dB and up to -36dB (all values below -36dB are depicted as the same dark blue color). The power drop front is quasi constant, with respect to the matching medium and moves right in a constant way with increasing frequency, revealing a similar attenuation over frequency independent of the matching medium's permittivity. Cuts for  $\epsilon_{mm} = 14, 56, 80$  of  $P_{Nt}$  are shown in the right picture of Fig. 2. It indicates that the power transmission is mainly affected by the tissue attenuation which is exponentially increasing with frequency. At 1GHz for example, the optimum is at  $\epsilon_{mm} = 10$ , however the normalized transmitted power drops by approximately 3dB if  $\epsilon_{mm} = 80$  (approximately water at 1GHz), but the imaging resolution would increase by almost a factor of 3. The same normalized transmitted power is obtained considering the field scattered by the anomaly and received by the probe. According to these observations, one can freely choose the permittivity of the matching medium with respect to power transmission. The critical parameter is the frequency that significantly influences the transmitted power. The almost free choice of the permittivity (1dB drop of  $P_{Nt}$  for increasing  $\epsilon_{mm}$  from 56 to 80) means also, that it can be used to improve the imaging resolution according to the discussion in the introduction. A good compromise for the frequency is around 1 GHz for which the attenuation in the head tissues is still acceptable.

### III. EXPERIMENTAL VALIDATION

#### A. Head Prototype

A 3D printed concentric multilayered spherical structure (see Fig. 3) has been manufactured. We used the Fused Deposition Modeling technology and white ABS (Acrylonitrile butadiene styrene) for the plastic.



(a) closed view

(b) opened view

*Figure 3: Pictures of the multilayered sphere prototype.*

The filling system consists of 5 entries, allowing to use a different liquid for each shell. The filling system and the holding system are designed in one piece to minimize its influence regarding the ideal multilayered concentric spherical model (Fig. 1 (right)) that we want to confront with measurements. Each of the entries has a blockage cap, 3D printed in a flexible material. The materials and thicknesses were designed to ensure waterproofness. The dielectric properties of the ABS plastic structure of the 3D printed prototype were measured in the range of  $[0.5 - 4]$  GHz using the Agilent 85070E dielectric probe kit. The relative permittivity is 2.6 and constant while the conductivity is negligible in the frequency range of interest. The plastic shells are 2mm thick. Several recipes are available to make liquids mimicking the main human head tissues. Following the guidelines adopted in [23], Triton X-100-water mixtures with NaCl (salt) (see Table 1) are used to emulate the targeted tissues.

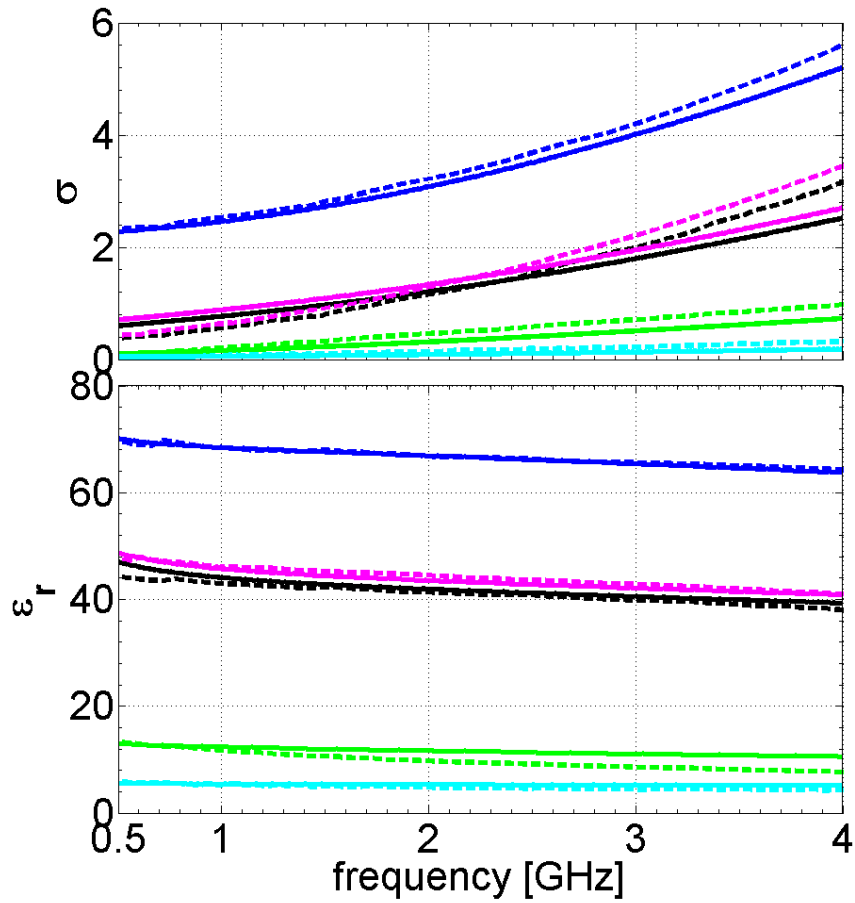


Figure 4: Theoretical (solid line) [12] and measured (dashed line) dielectric properties of the measurements of brain (black), CSF (dark blue), bone (green), fat (light blue) and skin (magenta).

The results for permittivity and conductivity measurements are depicted in Fig. 4, where the dispersive characteristics of their theoretical (targeted) values can be observed over the frequency band of interest.

Table 1: Triton X-100 and NaCl concentrations.

Tissue	Triton X-100 [%]	NaCl [g/L]	Thickness [mm]
Brain	35	4.3	43
CSF	7	14	3
Bone	85	0	7
Fat	100	0	4
Skin	30	4.3	4

## B. Measurement Results

The transmission parameter  $|S_{12}|$  between a monopole antenna (port 2) vertically placed in the center of the head phantom and a vertically polarized horn antenna (port 1) placed at 1m distance is measured between 0.5 and 4 GHz with a HP 8720D to ensure far field conditions of a linearly polarized plane wave, along the z-direction. As discussed in Section II, the matching medium is essentially useful to increase the imaging resolution, therefore measuring with a horn antenna in air is acceptable since the purpose of this simple setup is to experimentally validate only the power transmission inside the head computed by the analytical modeling tool.

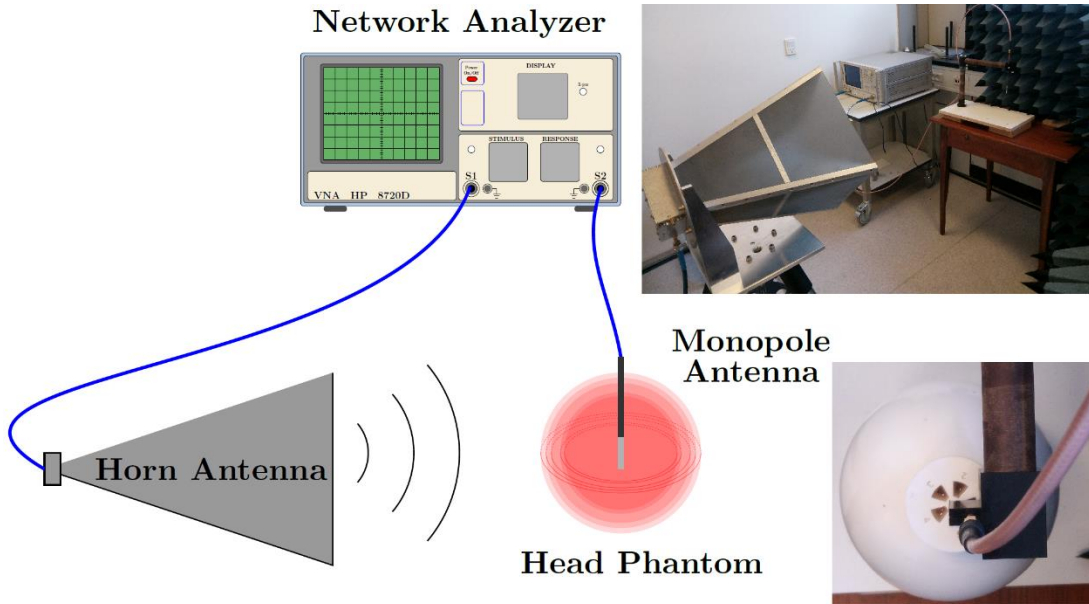


Figure 5: Schematic and picture of the measurement setup.

The measurements in the case of empty and filled spheres are denoted by  $S_{ij}^e$  and  $S_{ij}^f$  parameters, respectively. The ratio between these two measurements determines the amount of power injected into the brain from the horn antenna and is defined as the normalized transmitted power,

$$P_{Nt}(\omega) = F(\omega) \frac{|S_{12}^f(\omega)|^2}{|S_{12}^e(\omega)|^2} \quad \text{with} \quad F(\omega) = \frac{1 - |S_{22}^e(\omega)|^2}{1 - |S_{22}^f(\omega)|^2} \quad (2)$$

The coefficient  $F(\omega)$  enables to account the changing mismatch of the receiving monopole when immersed into the brain-mimicking mixture. The monopole, similar to the one used in [24] for breast imaging purposes with the only difference of a longer pin (4cm) to be adapted to the brain mimicking environment is well-matched over the entire measured frequency band (see Fig. 6).

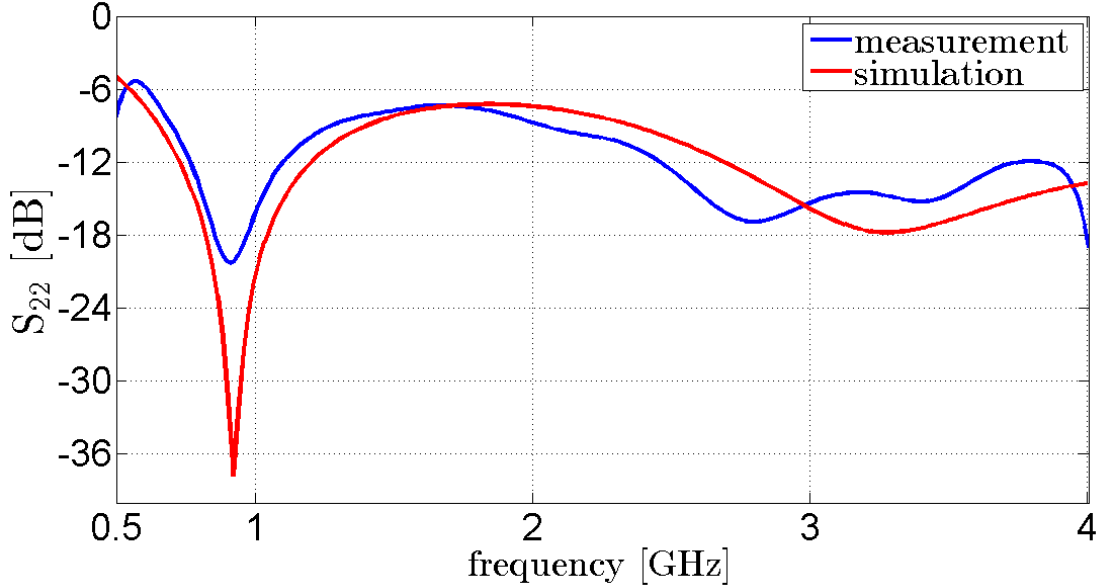


Figure 6: Monopole antenna specifications: measurement (blue) and simulation (red).

Additionally,  $S_{11}^f \approx S_{11}^e$  as the emitting horn antenna is in free space in both configurations. In Fig. 7 the measured normalized transmitted power is plotted in blue and compared to simulations obtained using the spherical model (in green, when  $\epsilon_{mm} = 1$  in Fig. 2 (left)).

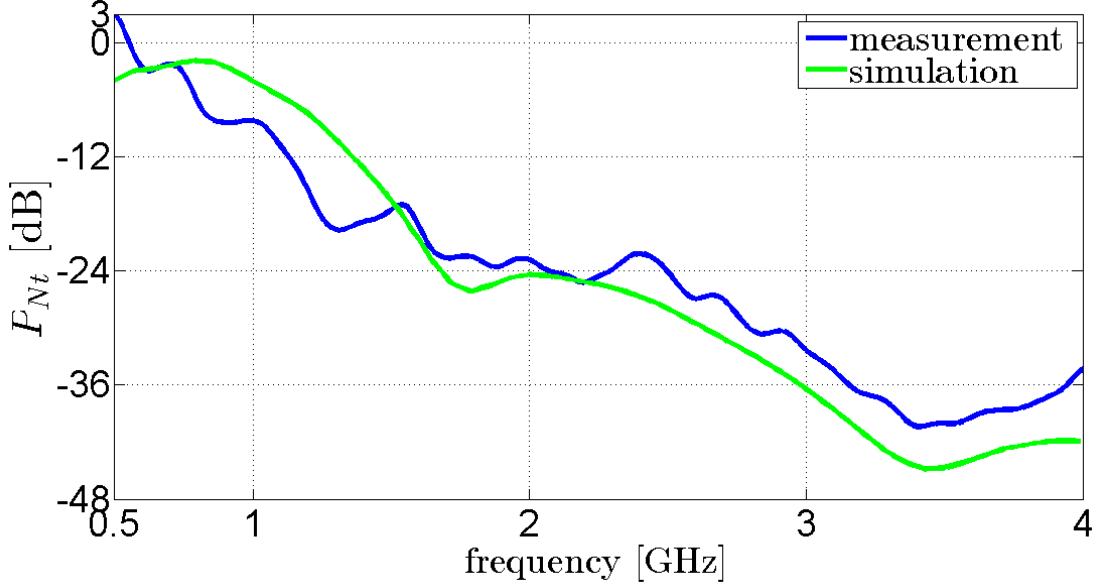


Figure 7: Normalized transmitted power as a function of the frequency: measured and simulated results.

One can easily observe that in the range [1.5 – 3]GHz the normalized transmitted power  $P_{Nt}$  drops very rapidly by 15dB due to the strong attenuation in the tissues, which was predicted by both the planar and the spherical model. This figure shows reasonable agreements between the measured and the simulated data of the same configurations. At 1.6GHz the normalized transmitted power is -17dB for both simulated and measured  $P_{Nt}$ . The difference of the normalized transmitted power of the simulations and the measurements can be explained by the difference of the targeted dielectric properties and the Triton-based mixtures (see Fig. 4) as well as the omission of the plastic layers in the numerical models.

As the filling process allowed to fill each layer on-site without moving the prototype (see Fig. 5), it was possible to estimate the influence of each layer on the power transmission. In Fig. 8 (upper part) are plotted ratios in dB of the  $n^{th}$  layer over the  $(n - 1)^{th}$  one, after the  $n^{th}$  layer is filled (from the brain to the skin layer). This power ratio  $R_n(\omega) = \frac{|S_{12}^n(\omega)|^2}{|S_{12}^{n-1}(\omega)|^2}$ , represents the propagation of the wave between the transmitting antenna (here the monopole antenna in the center of the brain region) and the surrounding environment in the case when only the core layer, representing the brain, is filled. In this representation 0dB means that there is no impact on the propagation of the wave, when an additional layer is added. If this ratio is positive

(green surface), it means that the added layer is beneficial to the propagation, or has a bad influence in the negative case (red region). It appears clearly that the “forbidden frequency band” observed in [14] around 2 GHz is mainly dictated by the layers of CSF and skin. The bone strongly cuts the propagation around 3 GHz, however, as the attenuation is high at those frequencies, this additional “forbidden band” is somehow hidden by the low levels of transmitted powers. The fat layer is good or neutral in the investigated frequency band. The frequencies for which the propagation is the most suited for imaging the brain is around 1 GHz. In the lower part of Fig.8, the product of all these influences gives the total influence  $R(\omega)$ , of all the layers on the wave propagation. It appears clearly that up to around 1.2GHz the “barrier” formed by the CSF, bone, fat and skin, is beneficial to the power transmission, and the opposite above this limit.

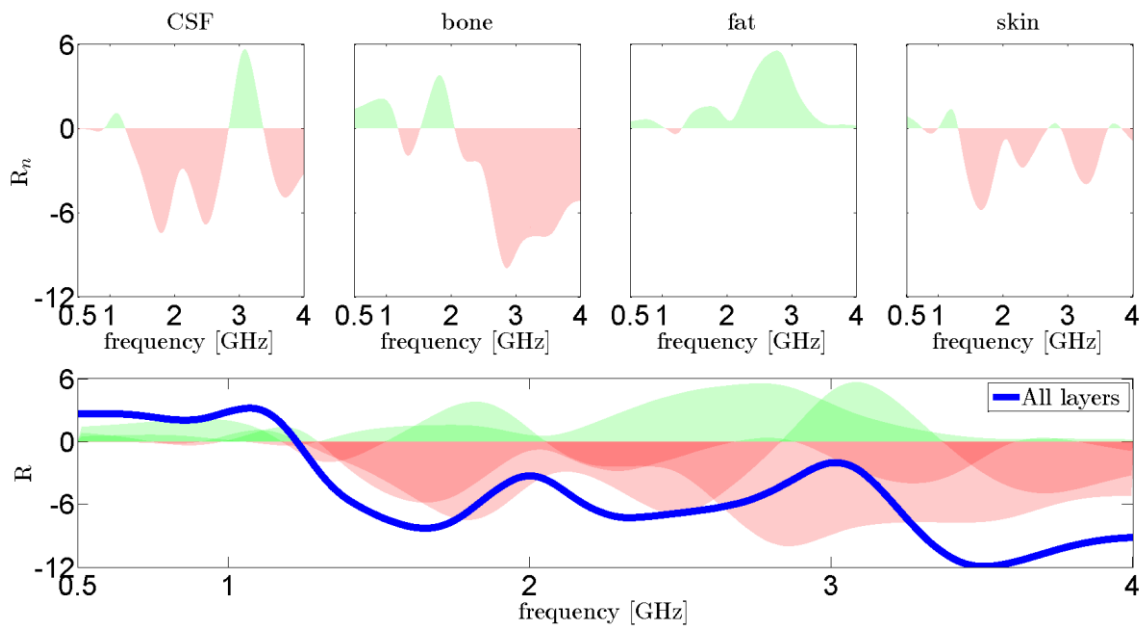


Figure 8: CSF, bone, fat and skin influences on the propagation.

#### IV. CONCLUSION

In this paper, the analysis of the normalized transmitted power of an impinging electromagnetic field onto a simplified model of the human head for MWI applications has been presented using a spherical multilayered model. Additionally, we presented a methodology to perform measurements outside and inside liquid phantoms using the 3D printing technology. The strong attenuation of at least 15dB between 1.5GHz and 3GHz in the measurements matches the predictions made with simple transmission line models [14]. It

confirms experimentally the trend to perform head MWI around 1GHz as the power attenuation is less than 10dB, for all considered matching media. The experimental results have been compared to theoretical results based on a spherical wave expansion and showed reasonable agreement. The background medium has a small influence on the power transmission into the brain and influences mainly the resolution of microwave imaging for a defined frequency, therefore one should choose a high permittivity. Moreover, the influence of the layers separating the imaging region (the brain) from the measurement setup on the propagation was qualitatively measured and analyzed. This information provides insight on the limit of the frequency, where this parameter starts to have a negative impact on the signal transmission between the brain and the matching medium, and therefore on the imaging quality. Depending on the sensitivity of the data acquisition of the imaging system, the frequency and matching medium ranges can be chosen using simplified analytical models and then be fine-tuned using more complex EM solvers and more realistic models of the head.

## **ACKNOWLEDGMENT**

This work has been supported by COST TD1301 MiMed and by the Swiss State Secretariat for Education, Research and Innovation under contract No. SBF1 C14.0071. Furthermore, we would like to thank Dr. Lorenzo Crocco and Dr. Rosa Scapatucci for the fruitful conversations and collaboration on the topic of MWI for brain stroke monitoring. We would also like to thank the EPFL-AFA and the DTU-EMS workshops for building, respectively, the prototype and the measurement setup.

## **REFERENCES**

- [1] M. Pastorino, «Microwave Imaging,» Wiley Series in Microwave and Optical Engineering. John Wiley & Sons, 2010.
- [2] R. Scapatucci, O. Bucci, I. Catapano et L. Crocco, «Differential microwave imaging for brain stroke followup,» *International Journal of Antennas and Propagation*, vol. Article ID 312528, p. 11, 2014.
- [3] A. J. Devaney, «Current research topics in diffraction tomography,» chez *Inverse Problems in Scattering and Imaging*, New York, M. Bertero and E. K. Pike, Eds. Adam Hilger, 1992, p. 47–58.

- [4] C. Pichot, L. Jofre, G. Peronnet and J. Bolomey, «Active microwave imaging of inhomogeneous bodies,» *IEEE Transactions on Antennas and Propagation*, vol. 33, n°14, p. 416–425, 1985.
- [5] F. C. Chen and W. C. Chew, «Experimental verification of super resolution in nonlinear inverse scattering,» *Appl. Phys. Lett.*, vol. 72, n°123, p. 3080–3082, 1998.
- [6] P. M. Meaney, K. D. Paulsen, A. Hartov and R. C. Crane, «Microwave imaging for tissue assessment: Initial evaluation in multitarget tissue equivalent phantoms,» *IEEE Transactions on Biomedical Engineering*, vol. 43, p. 878–890, 1996.
- [7] S. Y. Semenov, R. H. Svenson, A. E. Bulyshev, A. E. Souvorov, A. G. Nazarov, Y. E. Sizov, V. G. Posukh, A. V. Pavlovsky, P. N. Repin and a. G. P. Tatsis, «Spatial Resolution of Microwave Tomography for Detection of Myocardial Ischemia and Infarction—Experimental Study on Two-Dimensional Models,» *IEEE Transactions on Microwave Theory and Techniques*, vol. 48, n°14, pp. 538-544, 2000.
- [8] A. T. Mobashsher, A. Mahmoud and A. M. Abbosh, «Portable Wideband Microwave Imaging System for Intracranial Hemorrhage Detection Using Improved Back-projection Algorithm with Model of Effective Head Permittivity,» *Scientific Reports*, vol. Article number: 20459, n°16, 2016.
- [9] A. T. Mobashsher and A. M. Abbosh, «On-site Rapid Diagnosis of Intracranial Hematoma using Portable Multi-slice Microwave Imaging System,» *Scientific Reports*, vol. 6, p. 37620, 2016.
- [10] A. T. Mobashsher, K. S. Bialkowski, A. M. Abbosh and S. Crozier, «Design and Experimental Evaluation of a Non-Invasive Microwave Head Imaging System for Intracranial Haemorrhage Detection,» *PLoS ONE*, vol. 11, n°14, p. e0152351 <https://doi.org/10.1371/journal.pone.0152351>, 2016.
- [11] M. Persson, A. Fhager, H. D. Trefna, Y. Yu, T. McKelvey, G. Pegenius, J.-E. Karlsson and M. Elam, «Microwave-Based Stroke Diagnosis Making Global Prehospital Thrombolytic Treatment Possible,» *IEEE Transactions on Biomedical Engineering*, vol. 61, n°111, pp. 2806-2817, 2014.
- [12] A. T. Mobashsher and A. Abbosh, «Three dimensional human head phantom with realistic electrical properties and anatomy,» *IEEE Antennas and Wireless Propagation Letters*, vol. 13, p. 1401 – 1404, 2014.
- [13] S. Gabriel, R. W. Lau and C. Gabriel, «The dielectric properties of biological tissues: III. Parametric models for the dielectric spectrum,» *Physics in Medicine & Biology*, vol. 41, p. 2271–2293, 1996.
- [14] R. Scapatucci, L. D. Donato, I. Catapano and L. Crocco, «A feasibility study on microwave imaging for brain stroke monitoring,» *PIERB*, vol. 40, p. 305–324, 2012.
- [15] A. Moneda, M. Ioannidou and A. D. Chrissoulidis, «Radio-wave exposure of the human head: analytical study based on a versatile eccentric spheres model including a brain core and a pair of eyeballs,» *IEEE Transactions on Biomedical Engineering*, vol. 50, n°16, p. 667–676, 2003.
- [16] L. F. and C. S., «Electromagnetic fields inside a lossy, multilayered spherical head phantom excited by MRI coils: models and methods,» *Physics in Medicine & Biology*, vol. 49, p. 1835–1851, 2004.

- [17] M. Burfeindt, T. Colgan, R. Mays, J. Shea, N. Behdad, B. V. Veen and S. Hagness, «MRI-Derived 3-D-Printed Breast Phantom for Microwave Breast Imaging Validation,» in *IEEE Antennas and Wireless Propagation Letters*, vol. 11, p. 1610–1613, 2012.
- [18] N. Joachimowicz, C. Conessa, T. Henriksson and B. Duchêne, «Breast Phantoms for Microwave Imaging,» *IEEE Antennas and Wireless Propagation Letters*, vol. 13, n°11, p. 1333, 2014.
- [19] B. Guerin, J. P. Stockmann, M. Baboli, A. Torrado-Carvajal, A. V. Stenger and L. L. Wald, «Robust Time-Shifted Spoke Pulse Design in the Presence of Large B<sub>0</sub> Variations with Simultaneous Reduction of Through-Plane Dephasing, B<sub>11</sub> Effects, and the Specific Absorption Rate Using Parallel Transmission,» *Magnetic Resonance in Medicine*, vol. 76, p. 540–554, 2016.
- [20] N. Joachimowicz, B. Duchêne, C. Conessa and O. Meyer, «Reference Phantoms for Microwave Imaging,» *11th European Conference on Antennas and Propagation (EUCAP)*, Paris, 2017.
- [21] Y. Ge, R. Grossman, J. Babb, M. Rabin, L. Mannon and a. D. Kolson, «Correlations among Brain Gray Matter Volumes, Age, Gender, and Hemisphere in Healthy Individual,» *AJNR Am J Neuroradiol*, vol. 23, pp. 1327-1333, 2002.
- [22] R. A. Shore, «Scattering of an Electromagnetic Linearly Polarized Plane Wave by a Multilayered Sphere,» *IEEE Antennas & Propagation Magazine*, p. 69–116, 2015.
- [23] MiMed, «TD1301, COST Action MiMed. <http://cost-action-td1301.org>».
- [24] T. Rubæk, K. S. Oleksiy and P. Meincke, «Computational Validation of a 3-D Microwave Imaging System for Breast-Cancer Screening,» *IEEE Transactions on Antennas and Propagation*, vol. 57, n°17, pp. 2105-2115, 2009.
- [25] M. Slaney, A. C. Kak and L. E. Larsen, «Limitations of Imaging with First-Order Diffraction Tomography,» in *IEEE Transactions on Microwave Theory and Techniques*, vol. 32, n°18, p. 860–874, 1984.

**FIGURES (8=>2 pages)**

Figure 1: Spherical multilayered model to analyze the power transmitted into the human head..... 3

Figure 2: Normalized transmitted power according to the frequency [0.5-4]GHz, for a matching medium of  $\epsilon_{mm}=[1-80]$  (left). Cuts for  $\epsilon_{mm}=14,56,80$  of the  $P_{Nt}$  (right). ..... 4

Figure 3: Pictures of the multilayered sphere prototype..... 6

Figure 4: Theoretical (solid line) [12] and measured (dashed line) dielectric properties of the measurements of brain (black), CSF (dark blue), bone (green), fat (light blue) and skin (magenta)..... 7

Figure 5: Schematic and picture of the measurement setup. .... 8

Figure 6: Monopole antenna specifications: measurements (blue) and simulations (red). .... 9

Figure 7: Normalized transmitted power as a function of the frequency: measured and simulated results. 10

Figure 8: CSF, bone, fat and skin influences on the propagation..... 11